

A Comparison of Measured and Calculated Dynamic Aperture of the HERA Proton Ring at Injection Energy

O. Brüning*, W. Fischer, F. Schmidt and F. Willeke*

Abstract

We report on the measurement of the dynamic aperture in the HERA proton ring. The measurements are compared with tracking calculations. These calculations are based on a complex model of the accelerator using magnetic field measurements for each individual magnet in the ring. The simulation results reproduce reasonably well the measurements of dynamic aperture.

Geneva, Switzerland

June 6, 1995

* DESY Hamburg, Germany

Contents

1	Introduction	3
2	Preparation of the Accelerator and Physical Aperture	3
3	Numerical Calculation of the Dynamic Aperture	3
3.1	The Multipole Error Treatment in the Model	4
3.2	The Tracking Model	6
4	Comparison of Amplitude Dependent Tunes Measurements with Calculations	7
4.1	Measurement of the Detuning	7
4.2	Detuning in the Model	9
5	Dynamic Aperture	11
5.1	Experimental Dynamic Aperture	11
5.1.1	Dynamic Aperture obtained from Beam Losses	12
5.1.2	Dynamic Aperture obtained from Profile Measurements	14
5.2	Dynamic Aperture of the Model	15
6	Tune Ripple and its Compensation	18
7	Discussion	21
8	Acknowledgments	23

1 Introduction

The particle dynamics in the HERA proton ring suffers from strong nonlinear field errors at injection energy which limit the dynamic aperture. The source of the nonlinearities are the superconducting magnets. Persistent current field distortions play an important role, causing mainly systematic nonlinearities. Furthermore there are mechanical imperfections which distort the magnet geometry, producing randomly distributed nonlinearities. Furthermore, slow decay of the persistent currents and of the corresponding field errors creates additional problems, mainly operational ones. It also adds another source of random field errors since the decay varies considerably from one magnet to the other.

The field errors of the HERA proton ring are known in great detail. Each individual superconducting magnet has been cold tested. This included magnetic field measurements of at least two excitation levels and a recording of the persistent current decay. The results are described in several articles (see for example [1, 2]) and they are available from a database.

The dynamic aperture in the HERA proton ring at injection turned out to be tight but sufficient. For beams with an emittance in the range of $\varepsilon = (0.25 - 0.50)\pi$ mm mrad, beam life times of up to 10h could be achieved. No dedicated experiments on the dynamic aperture have been performed in the first years of HERA operation, however parasitic estimates of the dynamic aperture yielded acceptance values of only $A_x \simeq A_y < 1\pi$ mm mrad, which roughly is a factor of four less than expected from tracking calculations [6]. Since HERA has been operated with only up to 40% of its design intensity per bunch for the time being and since the beam emittance is expected to become larger for high intensity beams, there is a strong interest to carefully measure the dynamic aperture in the HERA proton ring. In the following we describe these measurements and the tracking calculations which have been performed in parallel.

2 Preparation of the Accelerator and Physical Aperture

The HERA machine has been carefully prepared for the experiments. In order to assure that the dynamic aperture is inside the physical aperture, a closed orbit correction has been carried out with orbit rms values below 2mm and no orbit deviation larger than 5mm. The full aperture in the regular sections is 27mm. Since the beam position monitors have unknown offsets in the order of (1-2)mm and since there may be alignment errors which further reduce the acceptance, the free aperture was optimized using the beam. The beam was displaced in both directions by short closed orbit bumps until a 80% loss occurred. Then the orbit was placed in the middle between the two extreme positions. The result of this tedious procedure was a horizontal acceptance of $A_x = 3.7\pi$ mm mrad and a vertical acceptance of $A_y = 2.5\pi$ mm mrad. The free horizontal aperture as obtained from these measurements is shown in Fig. 1. In order to avoid complication of the results by linear coupling, the width of the coupling resonance was compensated to a residual of $\kappa \simeq 2 \cdot 10^{-3}$. The chromaticity was measured and was kept to values between $\xi = 0$ and $\xi = 1$ in both planes. In order to provide constant conditions for the measurements, they were performed at injection energy and were started only one hour after the magnetic cycle was completed. After this time most of the persistent current decay has already taken place and one has almost constant operating conditions. The tunes have been chosen close to values used in normal operation with $Q_x = 31.285$ and $Q_y = 32.303$. All measurements were done with the standard injection beam optics.

3 Numerical Calculation of the Dynamic Aperture

The numerical calculation for the comparison was performed using the tracking code SIXTRACK [3]. This code allows the implementation of a detailed and realistic model of the accelerator. Magnetic field maps of each individual magnet can easily be included. There is sufficient flexibility to include additional effects like external tune modulation. As far as the tracking procedure is concerned, we closely followed a standardized

↑ Maximum Free Aperture

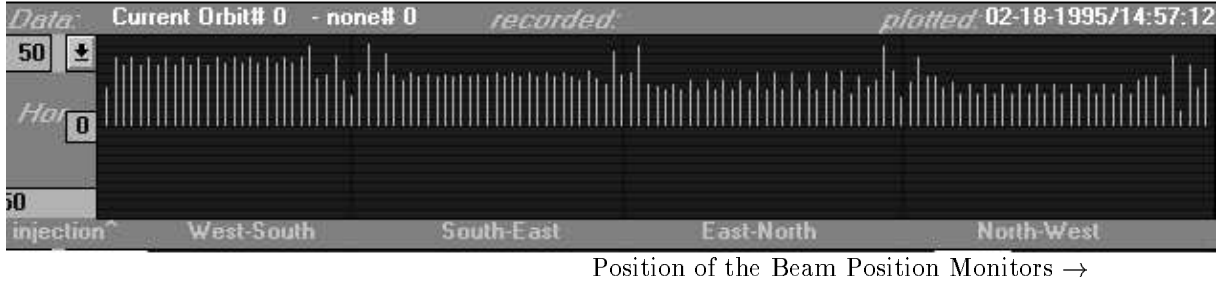


Figure 1: The Free Aperture in the HERA Proton Ring at the Positions of the Beam Position Monitors, the Nominal Aperture in the Arcs is $54mm$, the Vertical Full Scale is $\pm 50mm$

procedure as it is for example described in Ref. [4, 5]. We used the border to chaotic behavior as a conservative estimate of the dynamic aperture which is well confirmed by survival plots from long-term tracking.

3.1 The Multipole Error Treatment in the Model

For the multipole coefficients the notation according to the field expansion in cylindrical coordinates (r, θ, z) is used,

$$B_{\theta}(r, \theta) = B_{main} \sum_{n=1}^{\infty} \left(\frac{r}{r_0}\right)^{n-1} (b_n \cos n\theta + a_n \sin n\theta) \quad (1)$$

$$B_r(r, \theta) = B_{main} \sum_{n=1}^{\infty} \left(\frac{r}{r_0}\right)^{n-1} (-a_n \cos n\theta + b_n \sin n\theta), \quad (2)$$

B_{main} being the amplitude of the main field and $r_0 = 25mm$ the reference radius. The b_n are called “normal” and the a_n “skew” multipole coefficients respectively. The subscript “1” denotes a dipole, “2” a quadrupole etc. The multipole errors in the tracking model are based on measurements on each superconducting magnet [9, 11]. Great care has been taken to generate realistic magnetic field errors using the magnetic measurements. Measurements of multipole components may suffer from feed-down effects which are caused by a slightly misplaced measurement coil together with a strong dominant single multipole component. Furthermore, the measurements with the beam have extended over many hours, thus persistent currents had a long time to decay. This motivated the following procedure to generate the multipole errors used in the tracking. The geometric component of the multipole errors are taken from measurements at high excitation of the magnets (3000A). The persistent current part which is obtained from measurements at 250A excitation are overlaid. These values however have been corrected for persistent current decay using decay data for each individual magnet. For a few quadrupole magnets, the decay data are not complete. Here average values have been used which should not be of great importance. Strong persistent current decay occurs in the North and South quadrants of HERA. Therefore, the corrector currents of these machine parts were varied until a chromaticity of $\simeq 0$ was obtained. Table 1 shows the geometric part of the multipole errors and Table 2 lists the persistent current part of the multipole errors.

There is another effect which modifies the multipole field inside the magnets. If the main field changes, eddy currents are generated in the corrector coils wound on the beam pipe inside the magnets. The corresponding field distortions which affects the b_3 and b_5 values have been taken into account according to Ref. [12].

Table 1: Geometric part of the multipole errors, measured at 3000A, in units of 10^{-4} .

dipoles (422)									
	Italian (205)		German (217)			Italian (205)		German (217)	
	mean	rms	mean	rms		mean	rms	mean	rms
a_2	-0.421	2.011	-0.009	1.582	b_2	0.013	0.712	-0.034	0.459
a_3	-0.298	0.486	-0.256	0.303	b_3	-0.762	2.431	2.703	1.603
a_4	0.376	0.979	0.194	0.874	b_4	0.044	0.269	0.187	0.178
a_5	0.062	0.215	0.035	0.153	b_5	1.789	0.711	0.929	0.583
a_6	-0.168	0.244	-0.027	0.173	b_6	-0.016	0.115	-0.046	0.096
a_7	0.001	0.117	0.022	0.085	b_7	0.010	0.223	0.340	0.206
a_8	0.016	0.141	0.009	0.098	b_8	0.020	0.077	0.013	0.063
a_9	0.010	0.095	0.024	0.096	b_9	-0.309	0.119	-0.386	0.102
a_{10}	0.016	0.094	0.037	0.088	b_{10}	-0.035	0.098	-0.019	0.085

quadrupoles (224)									
	French (120)		German (104)			French (120)		German (104)	
	mean	rms	mean	rms		mean	rms	mean	rms
a_3	0.398	1.535	0.293	1.247	b_3	0.132	1.533	0.220	1.152
a_4	-0.084	0.990	0.021	0.862	b_4	0.183	0.599	0.017	0.781
a_5	0.060	0.492	-0.018	0.450	b_5	0.741	0.544	0.667	0.626
a_6	0.977	0.423	0.873	0.577	b_6	-2.662	1.226	-2.525	1.098
a_7	0.014	0.232	0.037	0.246	b_7	-0.010	0.216	0.014	0.190
a_8	-0.115	0.313	0.002	0.273	b_8	0.162	0.273	0.149	0.267
a_9	-0.018	0.352	-0.064	0.349	b_9	0.100	0.507	0.098	0.607
a_{10}	0.051	0.382	0.012	0.424	b_{10}	-1.606	0.395	-1.487	0.376

Table 2: Persistent current part of the multipole errors, measured at 250A, in units of 10^{-4} .

dipoles (422)									
	Italian (205)		German (217)			Italian (205)		German (217)	
	mean	rms	mean	rms		mean	rms	mean	rms
b_3	-34.013	1.422	-33.049	1.304	$\Delta b_3(1800s)$	3.218	0.599	1.798	0.454
b_5	10.777	0.734	11.195	0.862					
b_7	-2.360	0.422	-2.289	0.469					
b_9	0.786	0.457	0.801	0.470					

quadrupoles (224)									
	French (120)		German (104)			French (120)		German (104)	
	mean	rms	mean	rms		mean	rms	mean	rms
b_6	-21.362	1.054	-21.959	1.051	$\Delta b_6(1800s)$	0.967	0.225	1.003	0.185

3.2 The Tracking Model

The model of the accelerator used in our tracking calculation essentially agrees with the previously used model in [6]. However, compared to previous calculations, time dependent persistent current effects are taken into account in the description of the magnet field errors. Here is a brief description of the way the machine is represented in the input of the tracking code. Nonlinear forces are represented by thin lenses. In each half FODO cell (with a betatron phase advance of 45deg), there are eight thin lens kicks. The dipole magnets are split in three parts with two multipole lenses inserted in between. The quadrupoles are split in only two parts. The thin lenses carry the multipolar field errors as obtained from magnet measurements on dipole and quadrupole magnets up to order 10 (see Sec. 3.1) and they contain the effect of correction windings of sextupole, decapole and dodecapole correctors. The names of the thin lenses are different as they describe different correction settings for the North-, South-, East- and West-quadrants. The arrangement and naming of the the thin lens kicks is summarized in Fig. 2 and Tab. 3.

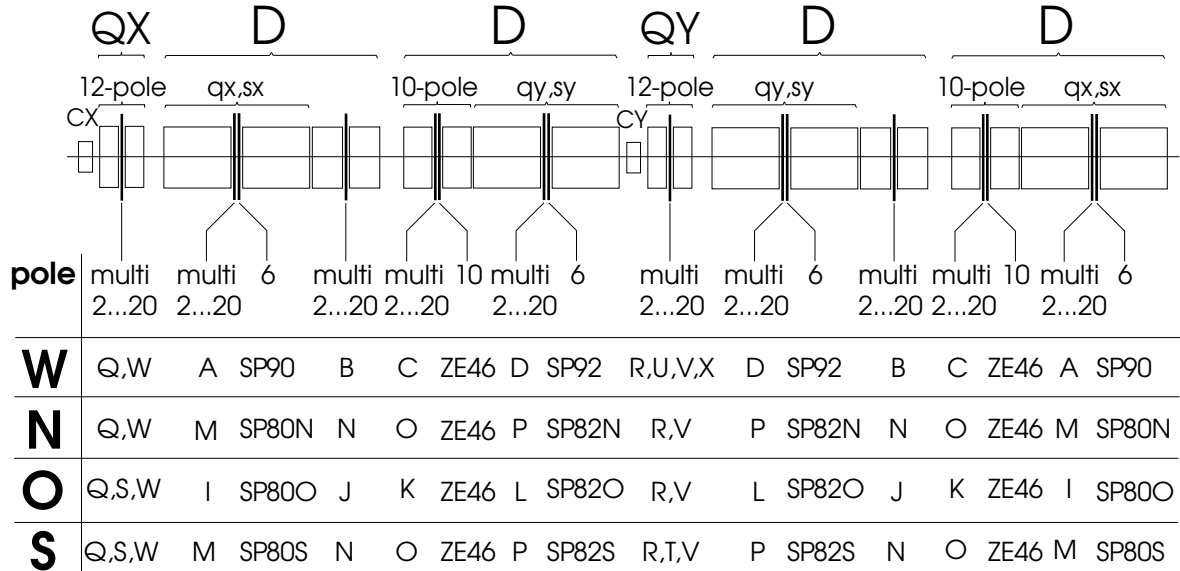


Figure 2: FODO cell of the HERA-p tracking model showing the positions and names of the nonlinear elements. CX and CY stand for horizontal and vertical dipole corrector respectively, qx and qz are tuning quadrupoles, sx and sy represent sextupole correctors.

The following adjustments have been performed for the model which are as similar as possible to the actual adjustments in HERA-p: tune, closed orbit, linear coupling, chromaticity and ripple. The nonzero closed orbit is generated by random dipole kicks in the multipole lenses. Simulations have been performed with corrected and uncorrected orbits whereas the orbit rms values are scaled to obtain the desired values. In a later version of the tracking code we used a closed orbit correction to obtain the desired level of residual orbit distortions and repeated some of the tracking calculations. No significant differences to the previous results were found. Linear coupling is generated by skew quadrupole components of the main field as obtained by the magnet measurements. The width of the coupling resonance is compensated to $\kappa \simeq 0.0015$ by using two single skew quadrupoles. The chromaticity is adjusted to a value of $\xi = \Delta Q / (\Delta p / p) \simeq 0$ using two sextupole families. Finally, harmonic tune modulation is introduced at 8 different azimuthal locations. The number of positions is a compromise between computing effort and the fact that a tune ripple is actually introduced by every element. This approach has been justified in [8].

Table 3: The different types of multipole lenses in the tracking model.

magnet type	multipole lens	purpose
dipole	A,B,C,D	WEST (German)
	M,N,O,P	NORTH and SOUTH (Italian)
	I,J,K,L	EAST (German)
	Y	vertical dipoles at IR's (German)
quadrupole	Q	type QX (French and German)
	R	type QY (French and German)
	S	type QX, no 12-pole corrector (French)
	T	type QY, no 12-pole corrector (German)
	U	type QU (German)
	V	type QV (German)
	W	type QW (German)
	X	type QU, no 12-pole corrector (German)

4 Comparison of Amplitude Dependent Tunes Measurements with Calculations

A nonlinear oscillator system is characterized by amplitude dependent tunes. Any localized nonlinear field in an accelerator will cause amplitude dependent tune. In HERA, the sextupole components of the superconducting magnets are a major contributor to this so called detuning. Since amplitude dependent tunes can be measured in an accelerator with much less ambiguity than the dynamic aperture and since they are an important characteristics of the nonlinearity, a comparison of measured and calculated detuning is a good check of a tracking model. Moreover, a tracking model can only be expected to reproduce the measured dynamic aperture if it reproduces the measured tune shifts with amplitude.

Using a Hamiltonian model, the detuning is described in the following way. If one assumes that one has transformed the usual accelerator coordinate system into a new system in which the phase dependent terms in the Hamiltonian are small enough to be neglected, the lowest order part of the nonlinear Hamiltonian has the form

$$H = aI_x^2 + 2bI_xI_y + cI_y^2, \quad (3)$$

where I_x and I_y are the horizontal and vertical action variables respectively and where a, b and c are the so-called detuning coefficients. The action variables are related to the Courant-Snyder emittance by the relation

$$2 \cdot I_{x,y} = \frac{1}{2\pi} \oint d\phi_{x,y} \varepsilon_{x,y} (\phi_{x,y}, \phi_{y,x} = \text{const}). \quad (4)$$

If the phase space is not strongly distorted by phase dependent terms, the detuning can be expressed simply by

$$\Delta Q_x = a\varepsilon_x + b\varepsilon_y, \quad (5)$$

$$\Delta Q_y = b\varepsilon_x + c\varepsilon_y, \quad (6)$$

where $\varepsilon_x = 2I_x$ and $\varepsilon_y = 2I_y$ are the horizontal and vertical emittance.

4.1 Measurement of the Detuning

In order to determine the detuning, the beam was kicked in one plane. The betatron oscillations for 1024 turns were recorded using the beam position monitor system. The tunes were determined by two methods, by FFT analysis and by calculating the phase advance from turn to turn using two beam position monitors spaced

by 90deg phase advance. This procedure was repeated with different kick amplitudes. Each measurement was performed with a fresh beam from the injector. In order to avoid a strong decay of the coherent signal by filamentation, the chromaticity was carefully compensated to $\xi_{x,y} \leq 1$. The orbit was well compensated with rms values of $x_{rms} \simeq z_{rms} \simeq 2\text{mm}$. Furthermore, before the beam was kicked, it was scraped until only about 20% of its original intensity was left over in order to avoid filamentation of the tails. The original Gaussian beam distribution with a σ of 2.3mm was reduced to a half foot width of $\simeq 1\text{mm}$. The injected beam current amounted to 0.2mA per bunch, which causes a space charge tune shift in the center of the bunch of $\Delta Q_{Laslett} = 0.0016$. For small amplitudes, the decay of the coherent betatron signal after 1024 turns amounted to about 50% (see also Fig. 3). Using several beam position monitors, this allowed the determination of the tune with a precision of about $\delta Q \simeq 5 \cdot 10^{-4}$. In order to excite the betatron oscillations in the horizontal plane, the injection kicker was used. The initial betatron amplitude was varied between $x_{ini} = 2.8\text{mm}$ at $\varepsilon_x = 0.07\pi$ mm mrad and $x_{ini} = 10.2\text{mm}$ at $\varepsilon_x = 1.5\pi$ mm mrad. Taking into account the final size of the beam, the outmost particles of the kicked beam had an emittance of up to $\simeq 2\pi$ mm mrad. In order to excite vertical betatron oscillations, the injection was mistuned. However, this was more difficult to control due to tight aperture constraints and coupling effects in the injection line. Therefore, only a few measurements could be performed. In order to test the sensitivity of the detuning with respect to changes in the decapole and dodecapole fields, the corresponding correction currents were varied as well.

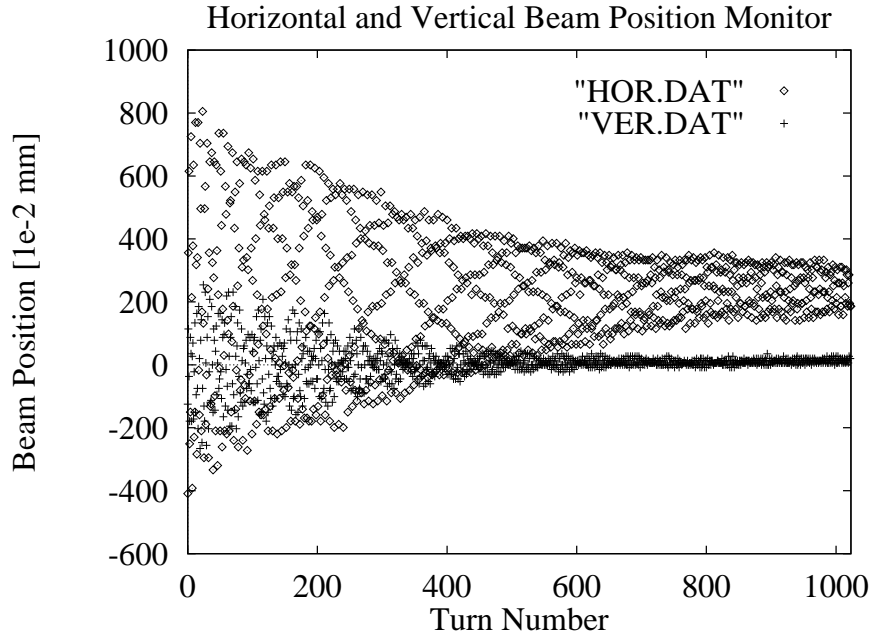


Figure 3: The signal in one of the position monitors after an 8kV kick, corresponding to an emittance of 0.3π mm mrad.

If the tunes of the excited beam are plotted versus the emittance associated with the betatron oscillation as shown in Fig. 4, it is apparent that the detuning is dominated by the lowest order terms. The detuning coefficients a and b may be determined from the slopes of the detuning curves by

$$a = \frac{\Delta Q_x}{\varepsilon_x}, \quad b = \frac{\Delta Q_y}{\varepsilon_x}. \quad (7)$$

A few measurements have been done to find the tune as a function of the vertical emittance (ε_y) using the injection line steering. Unfortunately, the beam was also oscillating in the horizontal plane (ε_x). The coefficients b and c are therefore calculated as follows:

$$b = \frac{\Delta Q_x - a\varepsilon_x}{\varepsilon_y}, \quad c = \frac{\Delta Q_y - b\varepsilon_x}{\varepsilon_y}. \quad (8)$$

The error bars in Fig. 4 are determined by taking different intervals and beam position monitors for the tune computation. Fitting a line to the experimental curve, one obtains $a = (3200 \pm 700)(\pi \text{ mm mrad})^{-1}$ and $b = (3600 \pm 1600)(\pi \text{ mm mrad})^{-1}$.

The excitation current of the 10-pole correctors ZE46 was changed from 30A to 15A. This corresponds to a change in b_5 of $3 \cdot 10^{-4}$ at $r=25\text{mm}$ in each dipole magnet ($\theta = 15\text{mrad}$). Furthermore the strength of the 12-pole correctors ZW44 was changed from 9A to 6A ($\Delta b_6 = 8 \cdot 10^{-4}$ at $r=25\text{mm}$ and $\theta = 1.49\text{mrad}$). These variations did not change the detuning within the measurement precision (Fig. 4). Since the detuning with amplitude depends only weakly on the 10-pole and the 12-pole correctors it can be concluded that the dominant contribution to the detuning comes from the sextupoles only.

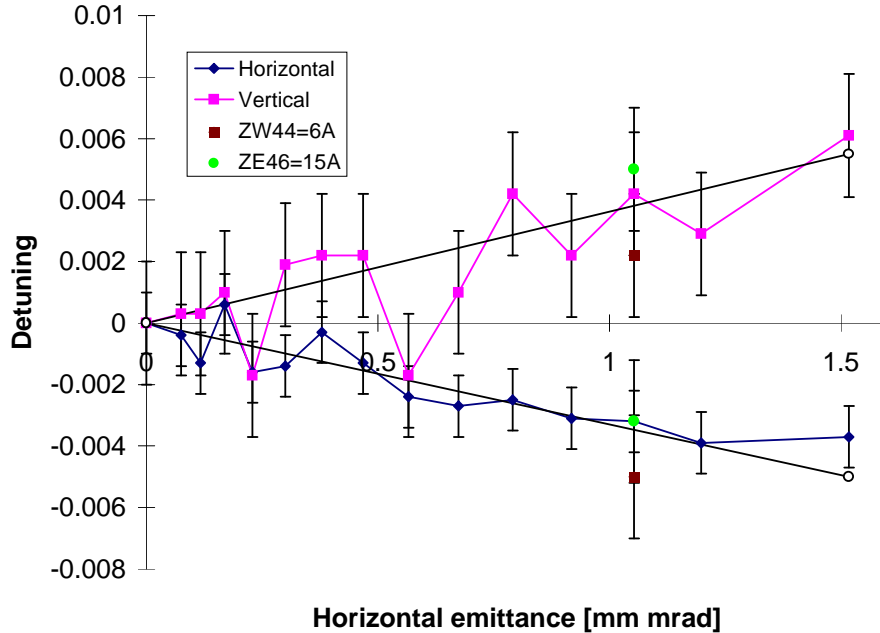


Figure 4: Measured tune changes as function of the horizontal betatron amplitude.

With the injection line steering there are only 3 measurements with small emittance values ($< 0.3\pi$ mm mrad) leading to $b = 6600 (\pi \text{ mm mrad})^{-1}$ and $c = 11400(\pi \text{ mm mrad})^{-1}$. However, these results are not very reliable because the measurements extends only over one fifth of the emittance range of the horizontal detuning measurement and have therefore a much larger error.

4.2 Detuning in the Model

In order to check the sensitivity of the detuning with respect to changes in the parameters of the model, these parameters were varied and the corresponding detuning was calculated. These variations were

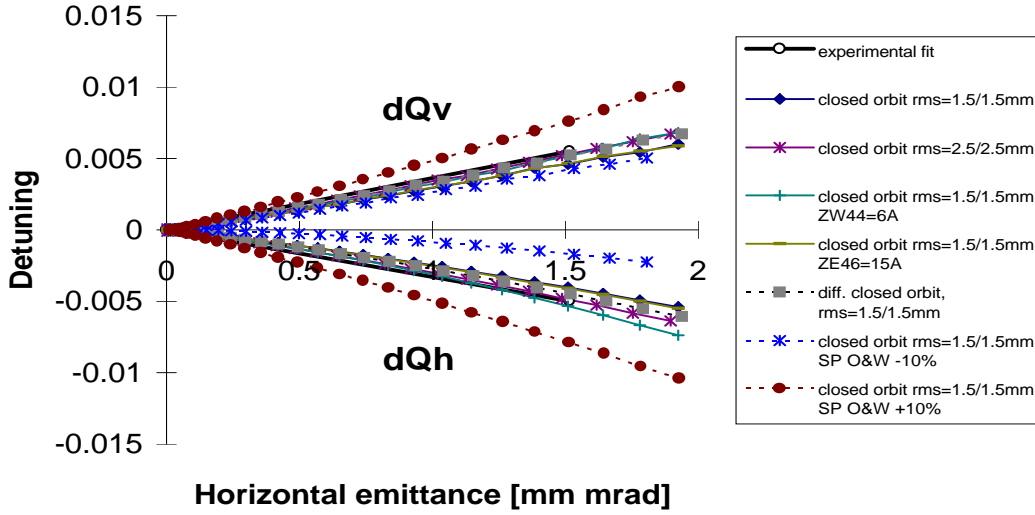


Figure 5: Detuning in the simulation for changing horizontal betatron amplitudes and parameters.

- closed orbit seeds
- closed orbit rms (1.5mm to 2.5mm)
(the orbit rms in the real machine is uncertain due to unknown offsets in the BPM readings with an rms of $\simeq 1$ mm.)
- closed orbit correction
- 10-pole and 12-pole corrector strength
- strength of the sextupoles in the East and West quadrants.

As mentioned above, the distribution of sextupole strength around the the superconducting accelerator has not been determined with complete certainty. The reason is the decay of the persistent currents which varies from magnet to magnet. We have to rely on the measurements on two reference magnets which should represent the magnets of the two half rings respectively. Because the control system in HERA-p allows only a global correction of the chromaticity, it is possible that there is some excess sextupole in one part of the machine which is compensated by the sextupoles in another part. The impact of such a variation on the detuning has been checked by calculation. A variation of the sextupole corrector values in the East & West quadrants by $\pm 5\%$ changes the detuning coefficient a by $\pm 35\%$.

Fig. 5 shows detuning results for the horizontal plane of the model and the fit to the experimental data. It turns out that only the variation of the sextupole distribution has a noticeable influence on the detuning. From the fact that the measured detuning curves coincide well with the calculated detuning obtained from the sextupole contribution taking into account the persistent current decay, one may conclude that the model reproduces well the distribution of the sextupole strength around the machine. The reference model used for the comparison of the dynamic aperture was chosen to return the proper detuning coefficient a . One then obtains for the coefficient $b = 3600(\pi \text{ mm mrad})^{-1}$ which is in perfect agreement with the measurement. The purely vertical term c comes out to be $5700(\pi \text{ mm mrad})^{-1}$ which is smaller than the measurement by almost a factor of two. However, the vertical detuning measurement is not very reliable. Fig. 6 shows the tune diagram for the experiment with resonances up to order 13 and the detuning according to the horizontal

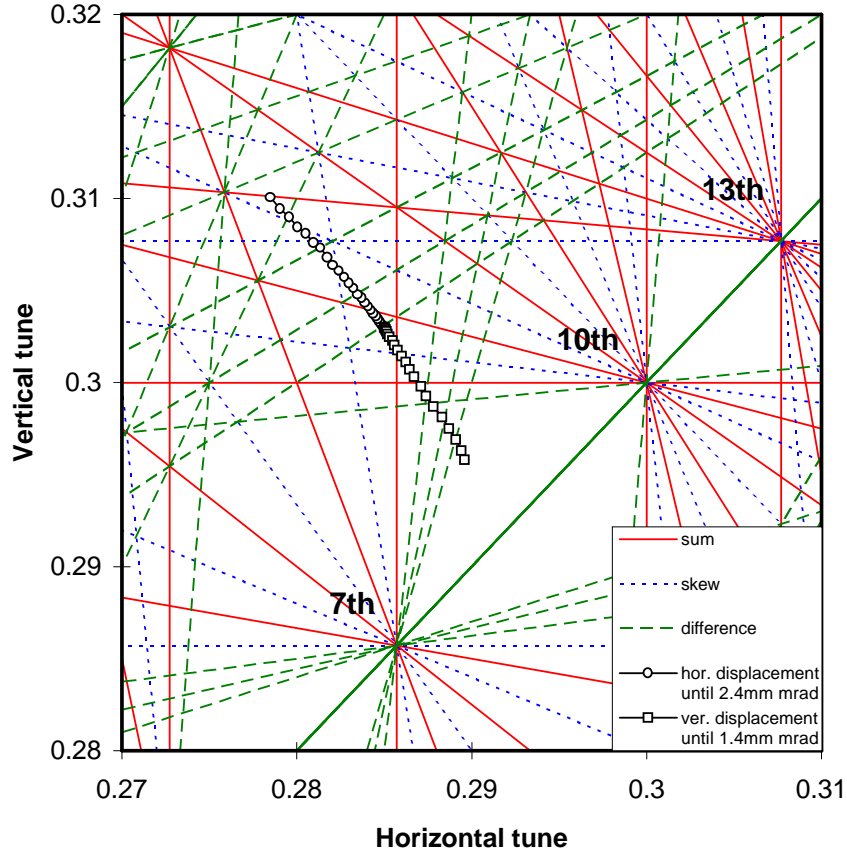


Figure 6: Tune diagram for the experiment. Resonances up to order 13 and the detuning according to horizontal and vertical betatron amplitudes is shown for the working point (31.285, 32.303). The detuning range corresponds to the beam size in the experiment.

and vertical betatron amplitudes for the working point (31.285, 32.303).

5 Dynamic Aperture

The definition of the dynamic aperture in the real machine is somewhat ambiguous. In the tracking model one might find stable trajectories and a more or less well defined border of stability. In a real accelerator one observes that there are no absolutely stable particles. This is due to the interference between nonlinear forces, noise, ripple, and scattering effects. A pragmatic approach is to define the dynamic aperture as the border inside which the particles remain within the initial amplitude for a certain time, for example the storage time. We required a stable particle to stay within its initial amplitude range for at least two minutes.

5.1 Experimental Dynamic Aperture

The dynamic aperture of HERA-p was studied at the injection energy of 40GeV. We used two methods to measure the dynamic aperture. In the first method we kicked a "pencil" beam and reconstructed the

edge of the stable region from beam loss measurements assuming an appropriate particle distribution inside the pencil beam. For the second measurement the beam was kicked so that it filled the available aperture and the dynamic aperture was observed as the foot width of the beam distribution. The conditions of the accelerator in these experiments were as described in the previous sections.

5.1.1 DYNAMIC APERTURE OBTAINED FROM BEAM LOSSES

The experimental setup was the same as for the measurement of the detuning coefficients. A single bunch with $3.3 \cdot 10^{10}$ protons and a normalized emittance $\varepsilon_N(2\sigma) = 7.8 \pi \text{ mm mrad}$ ($\sigma = 2.3\text{mm}$) was injected and scraped horizontally until only 20% of its original intensity was left. In order to interpret the data, knowledge of the transverse beam distribution is necessary. For the initial distribution we assumed a Gaussian distribution which is suggested by beam profile measurements made prior to the scraping. The beam distribution is then given by

$$\rho_1(x) = \frac{N}{\sqrt{2\pi}\sigma} \cdot e^{-x^2/2\sigma^2} \operatorname{erf}\left(\frac{\sqrt{\hat{x}^2 - x^2}}{\sigma}\right) \quad (9)$$

(\hat{x} is the scraper position and $\operatorname{erf}(x)$ is the error function.) The width of the distribution after scraping was about 4.2mm. The scraper was then retracted which takes about 60sec. Meanwhile the edge of the beam was softened by diffusion-like behavior of the particles. We modeled the corresponding tail by an additional contribution in form of a Gaussian distribution of width $\sigma = 2.3\text{mm}$

$$\rho_2(x) = \frac{N}{\sqrt{2\pi}\sigma} \cdot e^{-x^2/2\sigma^2} \quad (10)$$

so that the total distribution is

$$\rho(x) = (1 - \alpha)\rho_1(x) + \alpha\rho_2(x) \quad (11)$$

where α describes the population of the tails.

The beam was then kicked horizontally with the injection kicker and the whole procedure was repeated for different kick amplitudes. Fig. 7 shows the resulting current loss versus time for two different kick amplitudes.

The β -tron amplitudes of the beam centroid are between 8.4mm and 15.1mm which corresponds to emittances of $0.61\pi \text{ mm mrad}$ and $2\pi \text{ mm mrad}$. Due to coupling effects, the horizontal kick also excites vertical oscillations. Fig.3 shows that the vertical amplitude (normalized to the same β) amounts to 39% of the horizontal one. This vertical component has to be taken into account in the total betatron amplitude $a^2 = x^2 + y^2$. For the largest kick (18kV kicker amplitude), a β -tron oscillation amplitude of $a=16\text{mm}$ ($\beta = 115\text{m}$) or an emittance of $2.2\pi \text{ mm mrad}$ was excited. Then, more than 85% of the beam was lost two minutes after the kick. This means that most of the beam has been kicked outside the long term dynamic aperture. For the smallest kick ($U = 10\text{kV}$, $a=9\text{mm}$, $\varepsilon = 0.68\pi \text{ mm mrad}$), the beam loss is only marginal which means that most of the beam stays inside the dynamic aperture. The average kick strength gives a rough estimate of the dynamic aperture which is $a_x = 12.5\text{mm}$ or $A_x = 1.4\pi \text{ mm mrad}$.

The beam loss after the kick has been observed on time scales ranging from milliseconds to seconds. It is assumed that the particles are lost at the dynamic aperture border. Since the energy spread in the beam is small ($\Delta p/p \simeq 0.5 \cdot 10^{-4}$), we do not expect the aperture border to be significantly smeared out. Assuming these conditions and with the distribution function shown before, the beam losses translate into a dynamic aperture. If one waits long enough and if the assumed distribution is correct, the measurements with different kick amplitudes should all result in the same dynamic aperture. This requirement was used to adjust the population of the tails. It turns out that one has to assume an almost purely Gaussian distribution in order to achieve consistent dynamic aperture values from the different loss curves. The result of this procedure is shown in Fig. 8 and indicates a horizontal dynamic aperture of $a_x = 12.7\text{mm}$ or $A_x = 1.41\pi \text{ mm mrad}$.

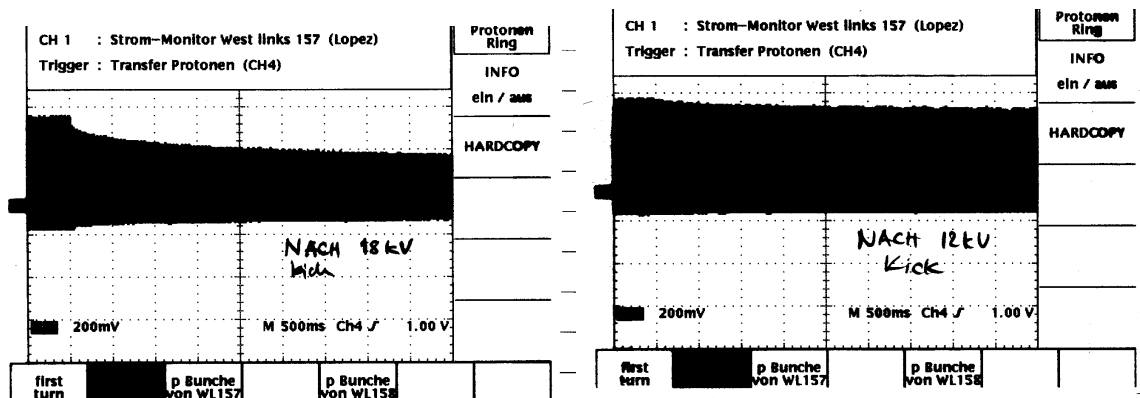


Figure 7: The current loss of the proton beam after a horizontal kick. Left-hand side: the current loss after a kick with 12kV amplitude. Right-hand side: the current loss after a kick with 18kV amplitude.

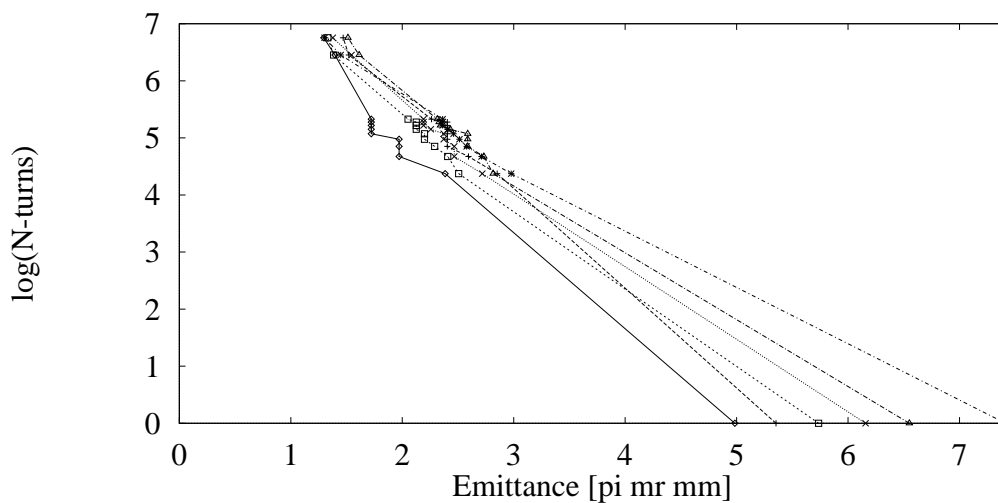


Figure 8: Horizontal Dynamic Aperture derived from Beam Loss Measurements

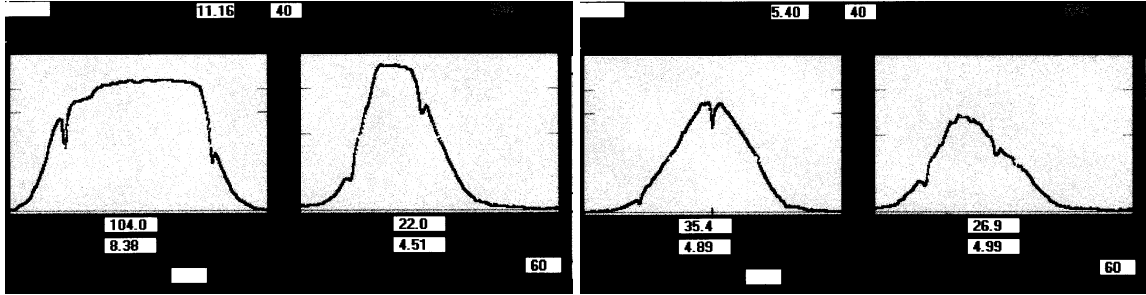


Figure 9: The beam profile at two different times after a horizontal kick. In both cases, the measurement was done with 60 bunches.

Left-hand side: the beam profile right after the kick.

Right-hand side: the beam profile 10min after the kick.

5.1.2 DYNAMIC APERTURE OBTAINED FROM PROFILE MEASUREMENTS

We worked with 60 bunches and a bunch intensity of $\simeq 2.5 \times 10^{10}$ protons per bunch. The measurements were performed in the following way. The beam was kicked horizontally with the injection kicker. The kick amplitude was chosen such that parts of the beam were lost at the physical or short term dynamic aperture limitation. This way, the beam filled the whole available aperture. The particles which were launched beyond the dynamic aperture were lost. Noticeable losses could be observed for about 10 minutes. A shrinking of the footwidth of the horizontal beam profile went along with particles losses. We identify the dynamic aperture as the edge of the shrunken beam distribution after 10 minutes.

Horizontal beam profiles have been recorded with a rest gas ionization monitor. This monitor has a time constant of about 0.5sec. Fig. 9 shows the beam profile at two different times after the horizontal kick. The left-hand side of Fig. 9 shows the beam profile right after the kick and the right-hand side 10min after the kick.

For the beam parameters under considerations, the systematic error of this monitor is small ($\leq 1\%$ error of the measured width) and its resolution of 0.1mm is sufficient. The β -function at this monitor amount to $\beta_x = 115\text{m}$ and $\beta_y = 157\text{m}$. All betatron amplitudes mentioned in this section refer to these β -values.

In Fig. 10 the results of six series of beam profile measurements are shown. The edge of the beam is shown as a function of time after the kick. The two rightmost curves in Fig. 10 are derived from measurements with a tune of (31.285, 32.303) (see Fig. 6 for the working diagram), with 60 bunches a 0.2mA and a residual beam current of (6-7)mA (after kick).

The edge of the beam distribution immediately after the horizontal kick is at 16.8mm. The last value corresponds to an emittance of about 2.4π mm mrad. Over a period of some 500sec the maximum horizontal amplitude decreases to 15.2mm, which corresponds to an emittance of 2.0π mm mrad. The error bars in Fig. 10 are determined from the uncertainty of reading the foot width of the rest gas monitor profile. Due to coupling effects, the motion excited by the injection kicker is not purely horizontal. The vertical beam profile which was observed simultaneously indicates that the initial vertical amplitudes after the kick amount up to 12mm.

The other cases were measured one day later and with only ten bunches. The beam was kicked with the injection kicker which reduced the intensity from 3mA to 1mA. The tunes were close to and inside the width of the coupling resonance at (31.287, 32.287).

In two cases an additional tune ripple of a depth of ($\Delta Q_x = 0.002$, $\Delta Q_y = 0.001$) was applied. In another case the existing tune modulation at frequencies of 100Hz, 300Hz and 600Hz were compensated. These cases will be discussed in the next section.

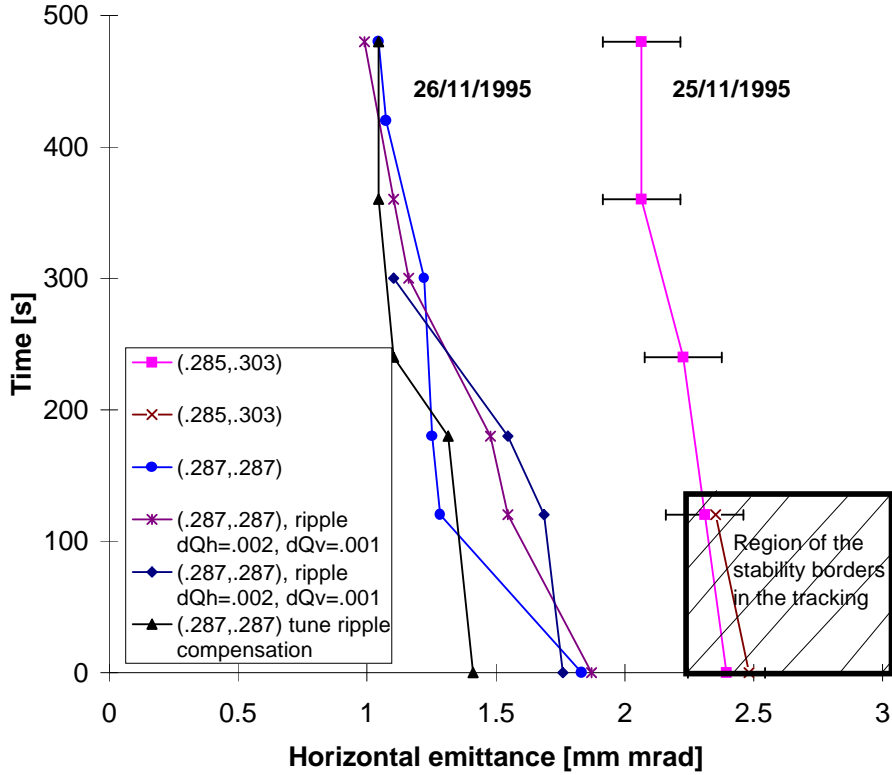


Figure 10: Horizontal Dynamic Aperture derived from Beam Profile Measurements

In all cases investigated, the measured horizontal edge of the beam distribution was significantly smaller than the day before. Since the beam was right on the coupling resonance, the initial horizontal and vertical β -tron oscillation amplitudes are expected to be equal. This is confirmed by the beam profiles after the kick. The edge of the beam immediately after the kick was found at 12.9mm horizontally and 13.2mm vertically. The emittance values which correspond to the beam edges are $\varepsilon_x = 1.45\pi$ mm mrad and $\varepsilon_y = 1.2\pi$ mm mrad. Ten minutes later the values are reduced to 10.7mm horizontally and 12.5mm vertically corresponding to emittance values of $\varepsilon_x = 1.0\pi$ mm mrad and $\varepsilon_y = 0.99\pi$ mm mrad.

5.2 Dynamic Aperture of the Model

The dynamic aperture of the model is computed by two methods: Firstly, the chaotic border is determined from the evolution of the distance of pairs of initially close-by particles, and secondly, by long-term tracking over 5 million turns. To get an upper bound for the dynamic aperture particles have been launched in the horizontal plane and vertical motion is only introduced through coupling. The momentum amplitudes were $\Delta p/p \simeq 1 \cdot 10^{-4}$ (0.66σ of the longitudinal distribution). The majority of the particles which are observed at the outer edge of the beam profile are represented by these parameters. It was checked by tracking whether particles with small momentum amplitude survive longer than particles with larger amplitudes. For the estimation of a lower bound (number in brackets in column six in Tab. 4), the vertical start amplitude was about 0.5σ .

Table 4 gives an overview for all tracking cases. The reference case (#1) has a modest closed orbit rms, a

Table 4: Particle stability in the tracking simulation. SP stands for the sextupole correctors, the stepsize for the detection of chaos is 0.18mm at $\beta_x \simeq 8.6\text{m}$ and 0.045mm for the long-term tracking. The number in brackets in column six gives a lower estimate for the dynamic aperture.

#	tune	closed orbit		remark	chaos onset at emittance [π mm mrad]	turns	loss at emittance [π mm mrad]	turns
		hor. rms [mm]	ver. rms [mm]					
0	.2850,.3030	0.0	0.0		3.02	$2 \cdot 10^4$	–	–
1	.2850,.3030	1.5	1.5	orbit corrected	(1.97) 2.84	$2 \cdot 10^5$	–	–
2	.2850,.3030	1.5	1.5	orbit uncorrected	3.20 3.00	$2 \cdot 10^4$ $2 \cdot 10^5$	3.05	$5 \cdot 10^6$
3	.2850,.3030	2.5	2.5	orbit uncorrected	2.72	$2 \cdot 10^4$	–	–
4	.2877,.2862	1.5	1.5	coupled, orbit corrected	3.11 ¹	$2 \cdot 10^5$	–	–
5	.2850,.3030	1.5	1.5	SP W&O +5% orbit corrected	(2.03) 2.55	$2 \cdot 10^5$	–	–
6	.2850,.3030	1.5	1.5	SP W&O +5% orbit uncorrected	2.56	$2 \cdot 10^4$	–	–
7	.2850,.3030	1.5	1.5	SP W&O -5% orbit corrected	(1.98) 3.19	$2 \cdot 10^5$	3.53	$5 \cdot 10^6$
8	.2850,.3030	1.5	1.5	SP W&O -5% orbit uncorrected	3.69	$2 \cdot 10^4$	–	–
9	.2850,.3030	1.5	1.5	tune ripple orbit corrected	(0.64) 2.60	$2 \cdot 10^4$ $2 \cdot 10^5$	–	–
10	.2850,.3030	1.5	1.5	tune ripple orbit uncorrected	2.76 2.56	$2 \cdot 10^4$ $2 \cdot 10^5$	2.69	$5 \cdot 10^6$
11	.2850,.3030	2.5	2.5	tune ripple orbit uncorrected	2.52	$2 \cdot 10^4$	2.51	$5 \cdot 10^6$
12	.2850,.3030	1.5	1.5	SP W&O +5%, tune ripple orbit uncorrected	2.36 2.16	$2 \cdot 10^4$ $2 \cdot 10^5$	2.30	$5 \cdot 10^6$

¹Here the emittance is given as $x_{max}^2/\beta_{nocoupling}$ where x_{max} is the maximum horizontal amplitude and $\beta_{nocoupling}$ the horizontal β -function for the uncoupled case.

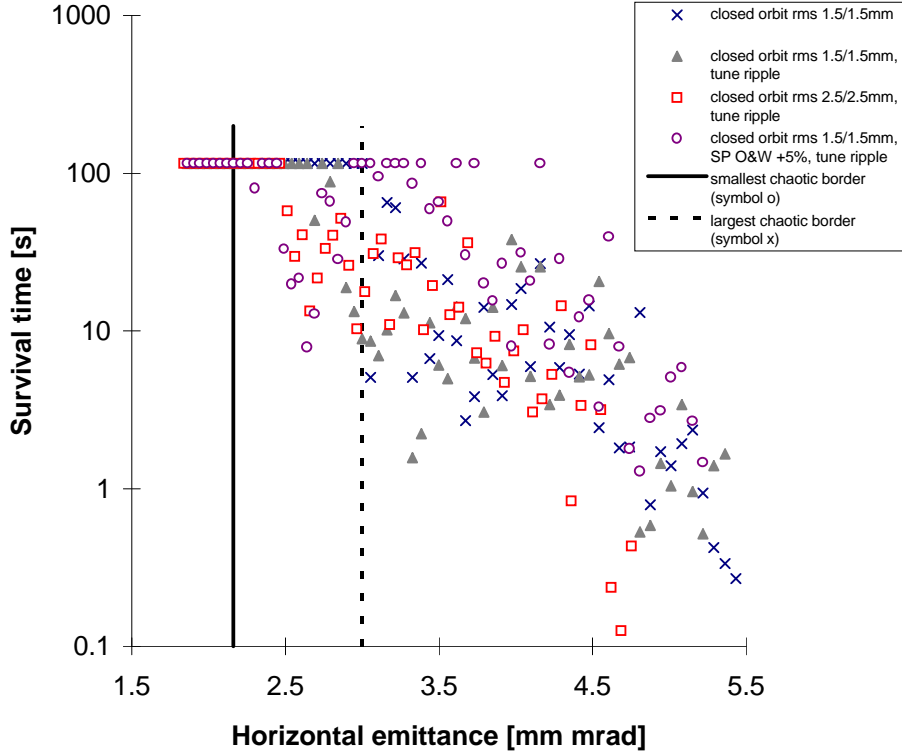


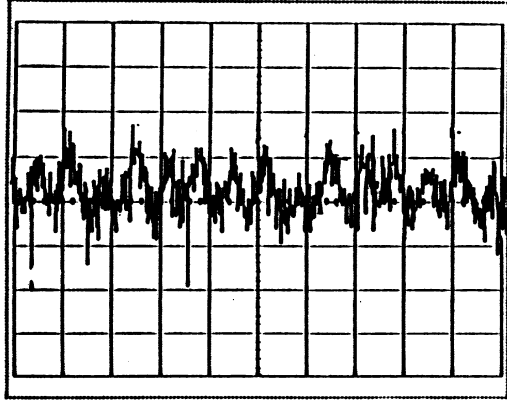
Figure 11: Survival plots for the cases #2, #10, #11 and #12 together with their smallest and largest chaotic border. SP stands for sextupoles correctors.

detuning that agrees with the experiment and no tune ripple. The other cases have the following properties: An uncorrected closed orbit (#2, #3, #6, #8, #10, #11, #12), a larger closed orbit rms (#3, #11), a stronger detuning (#5, #6, #12), a weaker detuning (#7, #8), tune ripple (#9 to #12) and finally different tunes (#4) with a coupled beam.

The table allows a qualitative differentiation between the various effects. The result barely depends on whether the closed orbit is obtained as a result of a correction process or not (compare #1 with #2, #5 with #6 and #7 with #8). The increase of closed orbit rms as well as the addition of tune ripple leads to a reduction of the dynamic aperture but both effects do not add up when combined. Increasing the detuning leads to an even larger reduction in the dynamic aperture, while decreasing the detuning increases the dynamic aperture by roughly the same amount. Finally, adding the tune ripple to the last case leads to a small further reduction of the stability border. Coupling does not seem to decrease the stable area (#4). In some cases (#2, #10 and #12) a Lyapunov analysis was done with turn numbers differing by a factor of 10. It is interesting to notice that in two cases with tune modulation (#10, #12) a region with clearly chaotic behavior has been discovered in an amplitude range well inside the dynamic aperture.

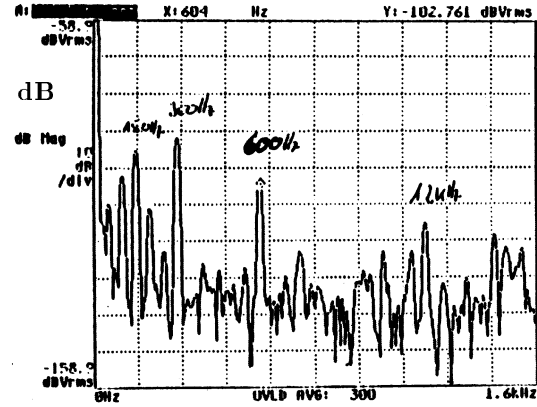
The survival plot (Fig. 11) shows four cases of Table 4 for which long-term tracking was performed. Losses between 0.1 and 100s of survival time are depicted together with their smallest and largest chaotic border. Particles which survive longer than 5 million turns build the upper straight line at about 105s.

↑ 1V/div.



→ t 5msec/div.

Power Spectrum



→ f[Hz]

Figure 12: The voltage ripple at the main proton power supply at injection energy (40GeV). The left-hand side shows the voltage ripple as a function of time and the right-hand side shows the power spectrum of the voltage ripple.

6 Tune Ripple and its Compensation

Tune modulation can lead to a reduction in the dynamic aperture of a storage ring and is expected to have a strong effect on the dynamic aperture of the proton storage ring in HERA [13]. In order to compare the measured dynamic aperture in HERA with the results from tracking calculations, one has to estimate the existing tune modulation in HERA and include the estimated modulation amplitudes in the tracking calculations. In the proton storage ring of HERA, there are four sources for tune modulation at injection energy (40GeV).

Power supply ripples lead to a tune modulation at multiples of 50Hz with modulation amplitudes of the order of $\Delta Q = 10^{-4}$. The ground motion in the HERA tunnel leads to a tune modulation with frequency components between 1Hz and 20Hz and with modulation amplitudes of the order of $\Delta Q = 10^{-5}$ [15]. Vibrations of the vacuum pumps lead to a tune modulation at 12Hz and 24Hz with modulation amplitudes of $\Delta Q \approx 10^{-5}$ [15]. And a non-vanishing chromaticity leads to a tune modulation at the synchrotron oscillation frequency. Typical modulation amplitudes in HERA due to a non-vanishing chromaticity are of the order of $\Delta Q \approx 10^{-5}$. For the following analysis only the tune modulation due to power supply ripples was considered and the resulting modulation depth was estimated in two different ways. First, the voltage ripple was measured directly at the power supply. The left-hand side of Fig. 12 shows the voltage ripple of the main power supply in HERA-p as a function of time. The right-hand side of Fig. 12 shows the corresponding power spectrum of the voltage ripple. Both measurements were done at the injection energy of 40GeV. The main dipole and quadrupole magnets of HERA are all connected in series and are powered by the same power supply. In order to avoid an overall dipole moment of the power circuit, the current flows first clockwise from the power supply through all the main dipoles, and then counter-clockwise through all the quadrupole magnets back to the power supply. The dipole chain is thus connected to the positive pole of the power supply and the quadrupole chain to the negative pole and the first magnets of both chains see voltage ripples of the same magnitude but with opposite sign. Table 5 lists the number superconducting magnets in the chain along with the inductivity and capacity values.

The resulting tune modulation can be obtained by putting the current ripple along the magnet chain in

Table 5: Inductivity and capacity of the superconducting magnets.

Magnet type	Number of Magnets	Inductivity / mH	Capacity / nF
quadrupole	224	5	46
dipole	422	60	85

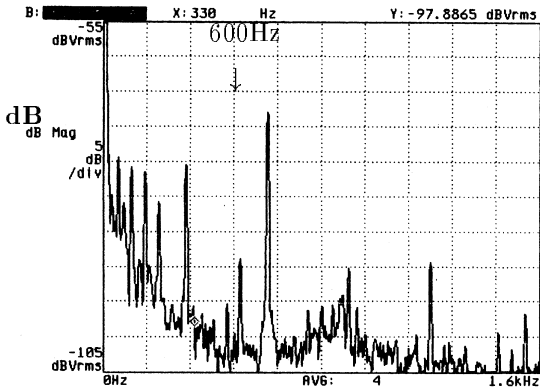
Table 6: The inferred tune modulation depths for the ripples in the main power supply of HERA-p.

Frequency [Hz]	50	100	150	200	300	600
ΔQ	$2 \cdot 10^{-5}$	$4 \cdot 10^{-5}$	$2 \cdot 10^{-5}$	$0.2 \cdot 10^{-5}$	$4 \cdot 10^{-5}$	$0.1 \cdot 10^{-5}$

an optics program like PETROS and taking into account the magnetic shielding of the thin copper layer in the vacuum chamber of the proton storage ring in HERA. Table 6 lists the resulting modulation amplitudes for the measured voltage ripple in Fig. 12.

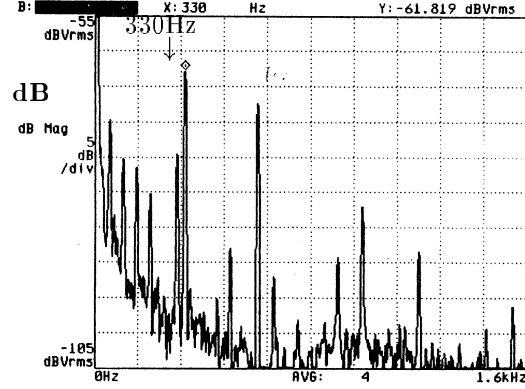
Alternatively, the tune modulation in the proton beam was measured with a phase-locked-loop (PLL). The PLL consists of a voltage-controlled oscillator (VCO), a transverse kicker in the proton beam and a pick-up. The signal from the beam pick-up is used as an input signal for the PLL and the output signal of the PLL is amplified and sent to a transverse excitation kicker. For a measurement of the tune modulation

Power Spectrum



$\rightarrow f[\text{Hz}]$

Power Spectrum



$\rightarrow f[\text{Hz}]$

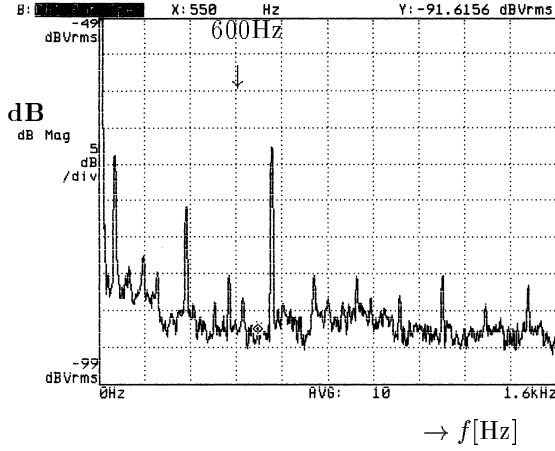
Figure 13: The tune modulation spectrum measured with a phase-locked-loop (PLL). The left-hand side shows the spectrum without any additional external tune modulation. The right-hand side shows the spectrum with an additional tune modulation with 330Hz and $\Delta Q = 3 \cdot 10^{-4}$. Both measurements were done at 40GeV.

in the proton beam, the difference signal of the VCO voltage and the pick-up signal is analyzed with a spectrum analyzer. Fig. 13 shows the power spectrum of two measurements at injection energy (40GeV). The left-hand side of Fig. 13 shows the power spectrum without an additional external tune modulation. The

Table 7: The tune modulation depths for the phase-locked-loop measurement.

Frequency [Hz]	50	100	150	200	300	600
ΔQ	$15 \cdot 10^{-5}$	$8 \cdot 10^{-5}$	$7 \cdot 10^{-5}$	$4 \cdot 10^{-5}$	$8 \cdot 10^{-5}$	$20 \cdot 10^{-5}$

Power Spectrum



Power Spectrum

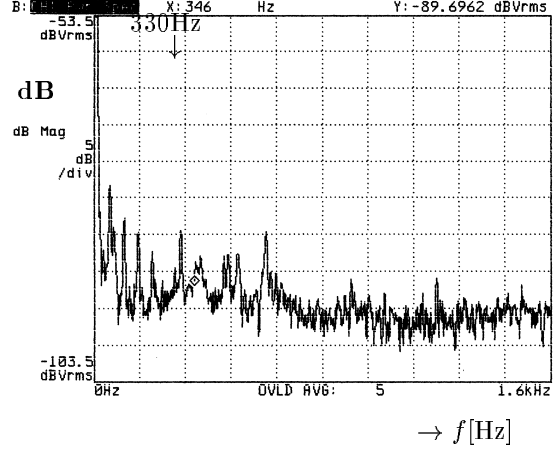


Figure 14: The tune modulation spectrum measured with a phase-locked-loop (PLL). The left-hand side shows the horizontal spectrum without an additional external tune modulation. The right-hand side shows the horizontal spectrum with compensated 300Hz and 600Hz lines.

right-hand side of Fig. 13 shows the power spectrum with an additional tune modulation with 330Hz and $\Delta Q = 3 \cdot 10^{-4}$. One clearly recognizes the typical 50Hz, 150Hz, 300Hz, and 600Hz ripple frequencies of the power supplies and their harmonics. The 330Hz line in the right-hand side of Fig. 13 was used to calibrate the frequency lines in the spectrum and Table 7 shows the resulting modulation amplitudes for the measured power spectrum in the right-hand side of Fig. 12. The measured modulation depths in Table 7 are all larger than the inferred modulation depths in Table 6, which indicates that either the ripple spectrum changes considerably with time, or that the frequency lines in the measured spectrum are not only caused by ripples in the main power supply. For example, other power supplies might contribute to the measured spectrum. The numerical particle tracking was done with the modulation depths from the PLL measurement.

The external tune modulation was generated by superimposing an ac-signal to the current in the superconducting correction quadrupoles of the proton ring. In order to analyze the effect of the tune modulation on the dynamic aperture experimentally, the dynamic aperture was measured with and without an additional external tune modulation. The external tune modulation can be either used to generate additional frequency lines in the tune modulation spectrum, or to compensate for individual frequency lines in the spectrum [17]. The dynamic aperture was measured for three different cases. First, the dynamic aperture was measured without any additional external tune modulation. In a second measurement, the tune modulation was used to compensate for the horizontal 100Hz, 300Hz, and part of the 600Hz lines. The left-hand side of Fig. 14 shows the spectrum of the horizontal PLL without an additional external tune modulation and the right-hand side shows the same spectrum with compensated 300Hz and 600Hz lines.

In a third step, the dynamic aperture was measured for an additional tune modulation with 50Hz and

a modulation depth of $\Delta Q \approx 2 \cdot 10^{-3}$. Fig. 10 summarizes these results. All three cases exhibit the same survival plot within the precision of the measurement.

7 Discussion

The comparison of measured and calculated tune shift indicates that the model which describes the accelerator is close to the real machine. The range of uncertainty of the parameters of the model produces a moderate variation of the detuning. The detuning for the most probable parameters agrees with the measurements.

The experimental values of the dynamic aperture suffer from the lack of control of the vertical oscillation amplitude. The reason for this is a local coupling which is left over after the global correction of the coupling with a single pair of skew quadrupoles.

In the case of the experiments with the pencil beam, the initial values of the vertical oscillation are very well known from turn-by-turn measurements of the beam position monitors. The maximum stable horizontal emittance derived from the beam losses is $A_x = 1.5\pi$ mm mrad. For a ratio of horizontal and vertical β -tron amplitude of 39% one obtains a dynamic aperture of $a=14.1$ mm or an acceptance of $A_x + A_y = 1.73\pi$ mm mrad. Unfortunately, these results depend on the assumed distribution. If the tails in the distribution are not taken into account, thus assuming the distribution of a scraped beam, the dynamic aperture values vary by a factor of 1.5 for different kick amplitudes. We eventually assumed a Gaussian distribution for which the values agree within a few percent. If one averages the dynamic aperture values from measurements with different kicks, the dependence of the distribution becomes small compared to other sources of errors. The fact that one has to assume tails in a beam distribution only about 60sec after scraping is thus not so relevant in obtaining a reliable value for the dynamic aperture, but it is an interesting fact itself. We will come back to this point below.

The evaluation of distribution functions of a horizontally kicked beam gives two different results for the stable edge of the beam. If the tunes are well separated and the working point is well outside the width of the coupling resonance the maximum horizontal amplitudes correspond to an emittance of about 2π mm mrad. It is somewhat problematic to estimate the associated vertical amplitude from the vertical beam profile. Except for the scraping, the experiment was performed in the same way as the experiment with the pencil beam and it appears to be justified to assume the same ratio for horizontal and vertical amplitudes. Thus the dynamic aperture obtained under these assumptions is $15.2\text{mm} \cdot \sqrt{1 + (0.39)^2} = 16.3\text{mm}$ which corresponds to an acceptance of $A_x + A_y = 2.32\pi$ mm mrad.

For the third measurement, the working point was chosen on the coupling resonance. Naively one expects under these circumstances that the maximum horizontal and the maximum vertical amplitudes in the beam after the kick agree and the dynamic aperture is $\sqrt{2}$ times the value which is obtained from the beam edge of the horizontal distribution, which would yield $a=15\text{mm}$ or an acceptance of $A_x + A_y = 2\pi$ mm mrad. This is certainly an upper value for the dynamic aperture compatible with this experiment.

All measurements have to be compared with the tracking results. If one first compares the shapes of the survival plots obtained from tracking and from the beam loss analysis (Figs 8 and 10) one finds them in qualitative agreement. Many particles survive up to a turn number of $5 \cdot 10^4$ (or 1sec). After this period there is a loss of large amplitude particles, which stabilizes after about 100sec.

The absolute values of the dynamic aperture only agree within 10%-20% if we assume that the correct model is the one which reproduces the detuning, the dynamic aperture from tracking is $a=18.6\text{mm}$ or $A_x + A_y = 3\pi$ mm mrad. The vertical start amplitude is zero, but there is some vertical amplitude exited by residual coupling in the model, which however was smaller than in the real machine. The results are summarized in Table 7. The discrepancies between tracking and measurements could be related to space charge effects. One has to take into account that single particles experience an additional strong space charge tune shift of $\Delta Q = 1.6 \cdot 10^{-3}$ which also translates into a tune spread or a tune shift with amplitude of the same size. If the beam is kicked as a whole, and filaments after a few thousand turns the charge density will be reduced and this additional tune shift with amplitude becomes also smaller provided that the amplitude

of the center of the kicked beam is larger than its size. This is true for the measurements with the scraped beam. (The detuning measurement should not be affected by the space charge since the corresponding coherent tune shift is small in HERA and is not amplitude dependent. The incoherent tune shift does not lead to additional filamentation.) The argument of reduced space charge tune shift is however not valid for the experiments with the unscraped beam. In this case the space charge tuneshift is only reduced by a factor of 2 or 3. The coefficient of the space charge tune shift with amplitude is expected to be $\Delta Q/\Delta\varepsilon = -250\text{m}^{-1}$. This changes the detuning values which are induced by the sextupoles by $\pm 10\%$ to $\pm 20\%$. The space charge induced tune shift with amplitude has not been taken into account in the tracking calculations. Since we know that a variation of the detuning strongly influences the dynamic aperture (see tracking cases #5 to #8), it is not unlikely that the space charge tune shift with amplitude is the reason for the modest discrepancy of the dynamic aperture values obtained from tracking and measurement respectively. If one compares the dynamic aperture values for the tracking cases with stronger detuning with the measured values ($a=16.3\text{mm}$) then one almost gets agreement with the best experimental values.

Table 8: Comparison of Dynamic Aperture Values from Experiment and Tracking

Analysis	Dynamic Aperture	Acceptance $A_x + A_z$	$\sqrt{A_y}/\sqrt{A_x}$	Q_x/Q_y
Tracking	18.6mm	3.00π mm mrad	$\simeq 0$.285/.303
Beam Loss	14.1mm	1.73π mm mrad	0.39	.285/.303
Beam Profile	16.3mm	2.32π mm mrad	0.39	.285/.303
Tracking	18.3mm	3.2π mm mrad	$\simeq 0.8$.287/.287
Beam Profile	15.0mm	2.00π mm mrad	$\simeq 1$.287/.287

The result that neither additional tune modulation of ($Q_{mod} = 2 \cdot 10^{-3}$) nor compensation of the most prominent existing tune modulation modes ($Q_{mod} \leq 10^{-4}$) had a noticeable influence on the dynamic aperture is surprising in view of the recent success in applying this procedure to high energy operation with beam-beam interaction [18]. Furthermore, theoretical estimates of the modulational diffusion (see e.g. [14]) indicate a rather strong effect of a tune modulation with modulation depths of 10^{-3} . The absence of any measurable effect for a tune modulation with modulation depths larger than 10^{-3} might indicate that the dynamic aperture at injection energy is not solely determined by tune modulation.

It should be noted at this point that measurements of the diffusion coefficients at injection energy are qualitatively different when compared to the results at high energy and beam-beam interaction. At high energy, experiments with scrapers suggest that the growth in the oscillation amplitudes is described well by a diffusion model with a diffusion constant which varies with amplitude. At injection, the gap which is created by a retracted beam collimator is filled much more quickly, as if there were a large number of particles with a rapid amplitude growth. It is not described by a diffusion model, since in a diffusion model the gap is filled more slowly and with steadily increasing speed [10]. The beam life time at injection is about 20 times smaller than at high energy with beam-beam interaction. The assumed population of the tail in the analysis of the beam loss experiments is at least qualitatively in agreement with the comparatively low beam lifetime. Analytically calculated diffusion rates due to interference of tune modulation with nonlinear resonances are orders of magnitudes are too low to explain the population of the tails at amplitudes of only a few millimeters.

Considering the available evidence, the required existence of tails to explain the beam loss experiments, the insensitivity of the dynamic aperture to tune modulation which is in contrast to analytical estimates and simulation, and the strong local nondiffusive amplitude growth observed with scraper experiments, one might argue that there is an additional mechanism which causes amplitude growth even near the central orbit, causes the poor life time, and might even reduce the dynamic aperture by enhanced amplitude growth

near the border of stability. However, such a source for particle diffusion at injection energy has not yet been identified and future efforts should concentrate on investigating possible sources of excitation.

8 Acknowledgments

The authors want to thank P. Schmüser and D. Gall for enlightening discussions and support for the multipole error treatment in the simulations. This study was only possible due to the commitment of the HERA operations crew.

References

- [1] P. Schmüser, “Field Quality Issues in Superconducting Magnets”, Proceedings of the 1991 IEEE Particle Accelerator Conference, San Francisco (1991), p 37ff.
- [2] H. Brück et. al., “Time Dependence of Persistent Current Effects in the Superconducting HERA Magnets”, DESY-HERA 90-01 (1990).
- [3] F. Schmidt, “SIXTRACK Version 1.2, Single Particle Tracking Code Treating Transverse Motion with Synchrotron Oscillations in a Symplectic Manner, User’s Reference Manual”, CERN SL/94-56 (AP) (1994).
- [4] F. Schmidt, “Sixtrack: A Single Particle Tracking Code”, Proceedings of the Workshop on Nonlinear Problems in Future Particle Accelerators, Capri (1990).
- [5] F. Galluccio and F. Schmidt, “Towards a Better Understanding of Slow Particle Losses in Large Hadron Colliders”, in AIP Conference Proceedings No. 225, Particle and Fields Series 48, Proceedings of the Advanced Beam Dynamics Workshop on Effects of Errors in Accelerators, their Diagnosis and Corrections, Corpus Christi (1991).
- [6] F. Zimmermann, “Dynamische Apertur und chaotische Teilchenbewegung im HERA-Protonenring”, DESY HERA 91-03 (1991).
- [7] I. Borchardt and P. Schmüser, “Polaritäten und elektrischer Verbindungen der supraleitenden Magnete und Korrekturspulen im HERA-Protonenring”, DESY HERA 93-01 (1993).
- [8] M. Furman and F. Schmidt, “Reduction of the Dynamical Aperture due to Tune Modulation”, CERN SPS/89-1 (AMS) and SSCL-A-6 (1989).
- [9] P. Schmüser, “Magnetic Measurements of the Superconducting HERA Magnets and Analysis of Systematic Errors”, DESY HERA-P 92-1 (1992).
- [10] M. Seidel, private communication.
- [11] D. Gall for the HERA magnet measurement group, private communication.
- [12] M. Pekeler, P. Schmüser and C. Stolzenburg, “Coupled Persistent-Current Effects in the HERA Dipoles and Beam Pipe Correction Coils”, DESY HERA 92-06 (1992).
- [13] F. Zimmermann, “Comparison of Calculated with Measured Dynamic Aperture”, SLAC-PUB-6504 (June 1994).
- [14] F. Zimmermann, “Transverse Proton Diffusion”, SLAC-PUB-6634 (October 1994).

- [15] W. Decking, “Zusammenhang zwischen Bodenbewegungen und der Strahlschwankungen in Speicherringen am Beispiel HERA”, DESY HERA 90-13 (1990).
- [16] H. Kaden, “Wirbelströme und Schirmung in der Nachrichtentechnik”, Berlin-Göttingen-Heidelberg (1959).
- [17] O. Brüning and F. Willeke, “Diffusion-like Processes in Proton Storage Rings due to the Combined Effect of Non-Linear Fields and Modulational Effects with more than one Frequency”, Proceedings of EPAC, London (1994).
- [18] O. Brüning and F. Willeke, to be published.